2nd URSI AT-RASC, Gran Canaria, 28 May – 1 June 2018

Characterization of nighttime polar ionospheric variability to solar and geomagnetic activity using wavelet analysis

Edith L. Macotela* (1), Mark Clilverd(2), and Jyrki Manninen(1)
(1) Sodankylä Geophysical Observatory, University of Oulu, Sodankylä, Finland.
(2) Space Weather and Atmosphere Team, British Antarctic Survey, Cambridge, UK.

Abstract

The very low frequency (VLF) radio wave technique provides the possibility of investigating the response of the lower ionosphere (~60-90 km) to a diversity of transient and long-term physical phenomena (e.g. solar activity). Monitoring average nighttime VLF measurements shows high variability that could be related to solar or geomagnetic activity. Thus, we aim to identify the periodicities that appear in the VLF measurements associated with changes in Lyman-α flux, solar wind velocity, and AE index. In this study, the powerful VLF signal transmitted from NAA (24 kHz) on the East Coast of the USA, and recorded at Sodankylä, Finland, was analyzed. We computed daily averages of the VLF, solar and geomagnetic data from April 2010 until December 2016. Then, the wavelet technique was applied to each one of the parameters. Our results show common periodicities of 374-408 and 25-33 days observed in the VLF measurements, Lyman-α flux, solar wind velocity, and AE index. We discuss the 25-33 periodicity in terms of the solar rotation rotation.

1. Introduction

Very Low Frequency (VLF: 3 – 30 kHz) radio signals propagate inside the Earth-ionosphere waveguide and can be used to monitor the electrical conductivity of its upper boundary whose electrical properties are represented by Wait's parameters [1], namely reference height (H_0) and conductivity gradient (β). The quiescent ionospheric condition can be disturbed by increases or decreases of ionization caused by solar [2] or terrestrial events like atmospheric waves [3].

Influence of the annual oscillation (AO) and semi-annual oscillation (SAO) in the nighttime VLF narrowband measurements were reported by Silber et al. [4] and Sharma et al. [5]. Silber et al. [4] used recorded VLF signals, that propagated in low- and mid-latitude regions, to determine the dominant oscillations in nighttime VLF measurements. They showed that the most dominant oscillation was ~180 days. The second dominant oscillation was ~343 days. The authors interpreted these oscillations in terms of the SAO and AO, respectively, suggesting that the SAO modulation in the VLF measurements were due to NOx transport. Another significant oscillation reported by Silber et al. [4] was a periodicity of 241 days (~8 months). However, no mechanism was suggested for this unexpected oscillation.

Sharma et al. [5] used recorded VLF signals, that propagated in mid-latitude regions to detect the SAO and AO oscillations. They applied the same method described by Silber et al. [4] and found that the nighttime VLF measurements exhibit more oscillations than just the SAO and AO. These other oscillations are of 111, 133, 151 and 217 days. However, the authors did not suggest any explanation for those oscillations. On the other hand, the studies of Silber et al. [4] and Sharma et al. [5] agree that the SAO is the strongest oscillation detected in the VLF measurements. Clearly, there is a lack of understanding of possible sources of induced oscillations observed in the nighttime VLF measurements.

The aim of the present study is to examine the nighttime VLF induced oscillations due to solar and geomagnetic activity. To determine the statistically significant periods, we employ the wavelet technique. In section 2 the data used in this work and the methodology applied for the analysis are presented. The obtained results are presented in section 3. The interpretation of the results and summary of the study are in the final section.

2. Data and methodology

To implement this study, two main data sets were used in the analysis: (i) data collected by a ground-based VLF receiver, and (ii) solar and geomagnetic data. An explanation of the data and methodology applied in the analysis are presented in this section.

2.1 Data

In this study, the narrow band subionospheric VLF data from a 24 kHz transmitter (call sign NAA, 44.6° N, 67.3° W) located in the East Coast of the USA and received at Sodankylä, Finland (SOD, 67.4° N, 26.7 E) were used. SOD is part of the Antarctic-Arctic Radiation-belt (Dynamic) Deposition - VLF Atmospheric Research Konsortium (AARDDVARK) network [6]. The VLF receiver at SOD is composed by two orthogonally orientated loop antennas, east-west and north-south.

In the study, NAA amplitude data from the east-west loop aerial recorded from April 2010 to December 2016 were used. Figure 1 shows the temporal evolution of the amplitude measured at SOD on 15 August 2010. The amplitude time profile illustrates deviations due to sunrise and sunset transitions over the VLF propagation path observed at 05 - 10 UT and 20 - 24 UT, respectively. The blue boxes in Figure 1 represent the time period used to compute the average 22 to 02 UT nighttime daily value.

Figure 2 shows the time series obtained after computed the daily average of the nighttime VLF amplitude of NAA received at SOD from 2010 until 2016. Missing measurements in Figure 2 occurred at times of transmitter or receiver maintenance.

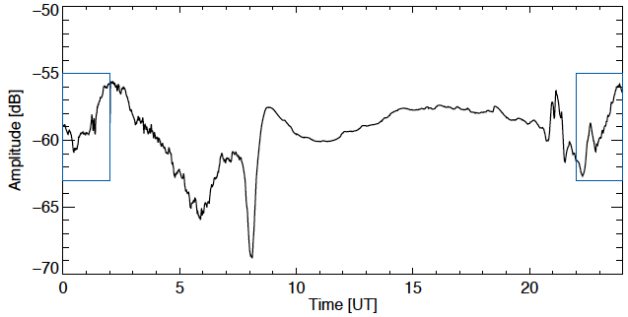

Figure 1. Diurnal amplitude variation of 24 kHz transmitted signal from NAA received at SOD on August 15th, 2010. The blue boxes represent the analysis time interval.

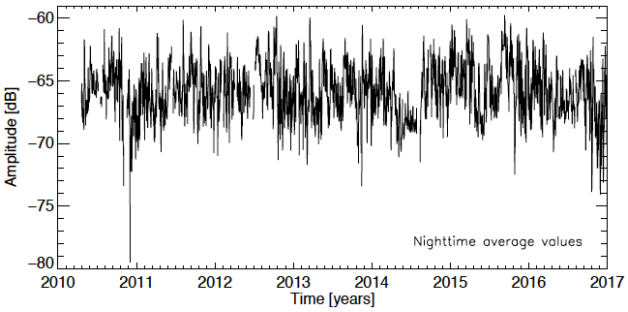

Figure 2. Temporal evolution of the daily average nightime VLF signal of 24 kHz transmission from USA (NAA) and received at Sodankylä (SOD), Finland.

To examine the nighttime VLF induced oscillations due to solar and geomagnetic activity we used the daily values of Lyman-α (Ly-α) flux, solar wind velocity, and AE index. These data were obtained from NASA/Goddard Space Flight Center's (GSFC) OMNI data set through the OMNIWeb interface (http://omniweb.gsfc.nasa.gov/).

2.2 Wavelet technique

Wavelet analysis is a tool for analyzing localized variations of power within a time series [7]. By decomposing a time series into time–frequency space, it is possible to determine both the dominant modes of variability and how those modes vary with time. The wavelet technique has mainly been applied to geophysical studies. Due to its benefits there are also potential applications to space weather studies [8].

In this study we have adopted the Morlet wavelet with a sampling time of 1 day. We compute the wavelet transform and the global wavelet spectrum. The global wavelet spectrum is the time-averaged power for every period found by the wavelet. To apply the wavelet technique requires the time series to be free of data gaps. Therefore, before applying the wavelet we filled the data daps with seasonally smoothed time series values. The results of the wavelet analysis applied to ionospheric, solar and geomagnetic variability are presented in the next section.

3. Results

Figure 3 shows in the upper panel the real part of the Morelet wavelet transform for the nighttime VLF analysis. The contours are the bipolar magnitude of the positive and negative matches between the phases of the wavelet and the time series. The color goes from dark blue to red. These colors indicate the maximum negative and positive magnitude, respectively. The black curve is the cone of influence, where the values above this curve are questionable. The global wavelet power spectrum for the nighttime VLF amplitude is showed in the lower panel. The dashed line is the 95% confidence level for the global wavelet spectrum. In both panels the red horizontal lines indicate the maximum of the significant peak periods. The peak periods are identified as 408, 187, 86, 33 and 14 days.

The upper panel of Figure 3 exhibits as contours the temporal evolution of all periods found by the nighttime VLF wavelet analysis. Observing the bands around the significant periods displayed in the lower panel of Figure 3, we notice a decreasing trend from 408 to 200 day period after 2015. Thus, the 408 day period exists until the end of 2014, being strongest between the years 2013 and 2015. The 187 day period, it appears over all of the analyzed years, with strong magnitude from late 2014 until early 2016. However, the 86 day period appears during 2011 with very weak magnitude, in late 2013 with weak magnitude, and during all of 2015 with strong magnitude. However, around this periodicity there is a decreasing trend from period just above 100 day to ~60 day. The 33 day period is observed over the analyzed years with strong magnitude in late 2011, early 2013 and late 2015. In the case of the 14 day period, it is more likely to appear during winter time with strongest amplitude in early 2012 and late 2016.

The format of Figure 4 is the same as in Figure 3, but for Ly-α flux. The significant peak periods in Figure 4 are at 374, 222, and 25 days. Tracking the contours of these periods (upper panel of Figure 4) we observe that the 374 day period can be clearly identified from 2013 with consistent magnitude. The contours for the 222 day period

disappears after 2013 until 2015. After 2015 this period is observable but weak. In the case of the 25 day period, its contours can be observed during all of the years analyzed, only disappearing during short periods of time in 2010, 2011, 2012 and 2016.

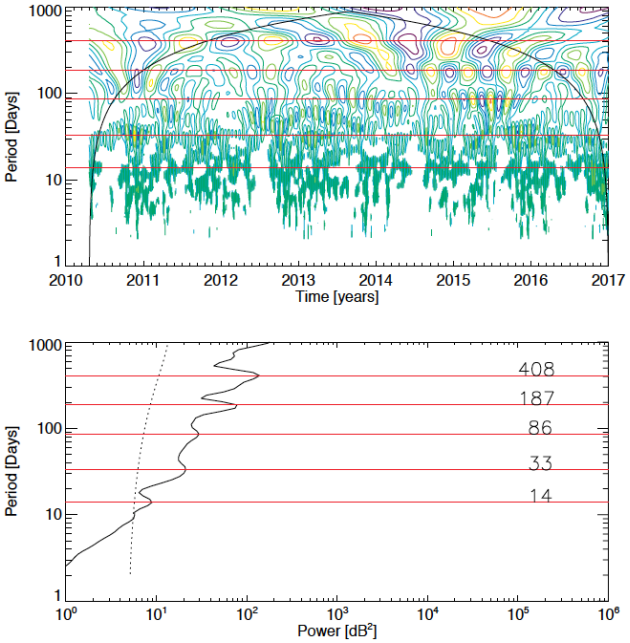

Figure 3. Contours of the real part of the wavelet transform of the daily nighttime VLF amplitude in the time-period domain (upper panel). The contours colors indicate the maximum negative (dark blue) and positive (red) magnitude of the matches between the phases of the wavelet and the time series. The black curve is the cone of influence. The global wavelet power spectrum is showed in the lower panel. The dashed line is the 95% confidence level for the global wavelet spectrum. The red horizontal lines indicate the maximum of the significant peak periods which are at 408, 187, 86, 33 and 14 days.

The format of Figure 5 is as in Figure 3, but for solar wind velocity. The significant peak periods in Figure 5 are at 343, 94, 47, 28 and 14 days. We observe that the peak around 343 days does not show clear contours. The center of the contours is at a slightly higher period around 2012, with strong magnitude, and in a slightly lower period between 2014 and 2016, with weak magnitude. Oscillations with a periodicity of 94 days appear in 2013 and 2015. Periods of 47, 28 and 14 days can be observed from 2010 until 2016 with absence during short periods of time. Contours of period 24 have strong magnitudes in 2010, 2013, 2015 and 2016.

Figure 6 description is the same as in Figure 3, but for the AE-index. The significant peak periods in Figure 6 are at 374, 28, and 14 days. In this figure, the 374 day period shows a well defined contour band. However, after 2014 the magnitude at this period is weak. The 28 day period appears sporadically before mid 2014 and more continuously after that time. This periodicity has a strong contour before 2016. The 14 day period is irregularly observed, with a strong contour in late 2016.

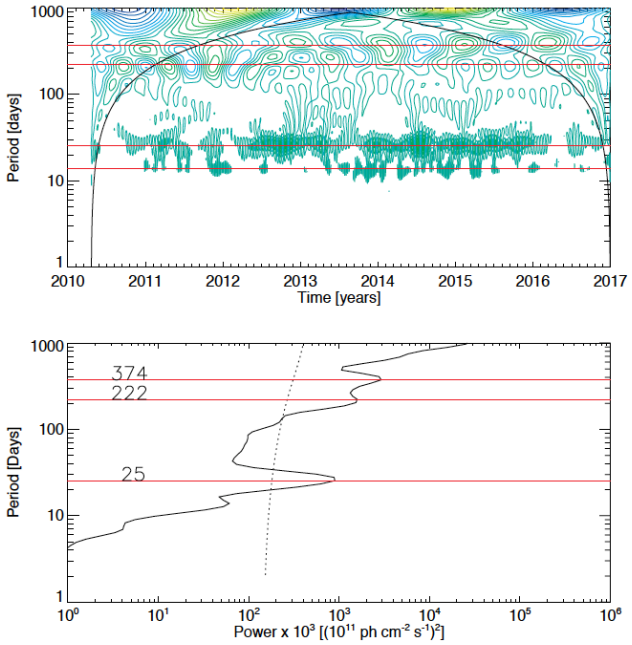

Figure 4. As described in Figure 3 but for Ly-α flux wavelet analysis.

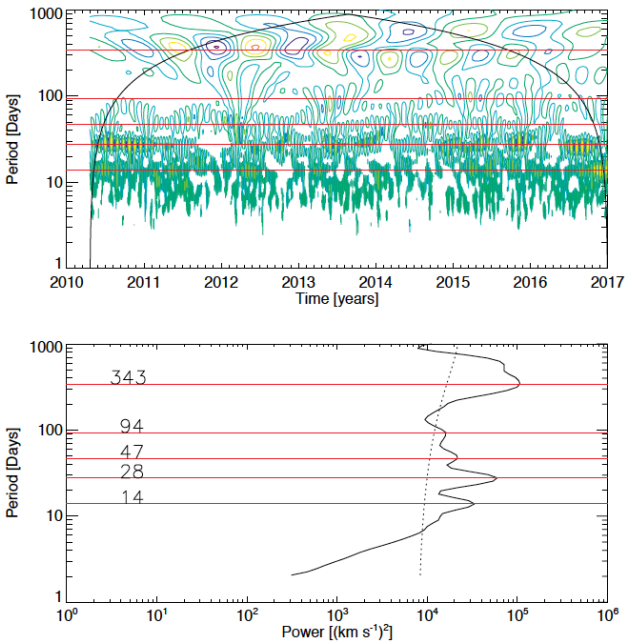

Figure 5. As described in Figure 3 but for solar wind velocity wavelet analysis.

From Figure 3, 4, 5 and 6 we observe that the common periodicities that appear in all the analyzed parameters are periods of 374-408 and 25-33 days. The power of the periods in the global wavelet spectrum are tricky to compare. However, the occurrence characteristics of the periodicities, observed with different parameters, can help to clarify the relative roles of each external driver on the VLF nighttime propagation.

4. Discussions and Summary

In this study, oscillations due to solar and geomagnetic activity induced in the nighttime VLF measurements are examined by wavelet analysis. This technique has the advantage of determining both the dominant periods of variability and how those periods vary in time. The VLF data which were used is the amplitude of the VLF signals emitted by the NAA transmitter recorded in Finland. The solar and geomagnetic activity data were obtained with a time resolution of one day through the OMNIWeb interface.

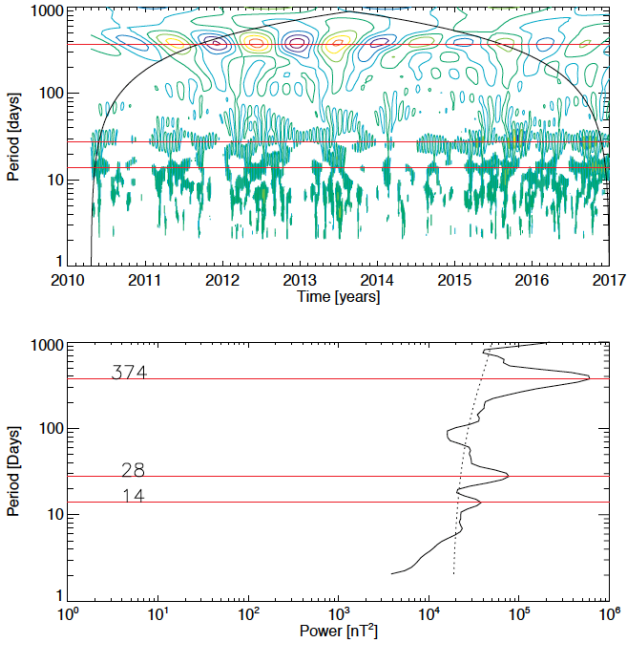

Figure 6. As described in Figure 3 but for AE index wavelet analysis.

The main result of this study is the following: common periodicities appearing in all the analyzed parameters are in the range 25-33 and 374-408 days. The 25-33 day periodicity can be interpreted as the induced oscillation due to solar rotation. For solar wind and geomagnetic parameters, the 374-408 day periodicity could be related to Earth's orbital motion in a latitudinally asymmetric solar wind as suggested by Zieger and Mursula [9].

Solar wind also shows a weak 94 day period which is seen co-incidentally in the VLF, but the weak 47 day solar wind period is not isolated in the VLF wavelet analysis. It is possible that the ~90 day and ~45 day periods in the solar wind are harmonics of the quasi-AO found in the solar wind analysis. However, the behavior of the VLF data around these periods is complex, and may be linked mechanisms other than the solar wind driver.

AE shows a strong AO, as well as the solar rotation period, and looks to be a strong influence on the VLF. The VLF could have some additional AO contribution from the solar wind at solar maximum (2011-2013), and scattered Ly-alpha in the declining phase of the solar cycle (from 2014 onwards). Scattered Ly-alpha may also have a contribution to the VLF response at the 25-30 day solar rotational period, particularly during the declining phase of the solar cycle. None of the driving-factors analyzed clearly showed the SAO, although it is present in the nighttime VLF data. The declining phase occurrence characteristics of the SAO in the VLF data maybe due to seasonal transport of NOx as suggested by previous work. Analysis of additional datasets might help clarify this mechanism, i.e., NOx, Ap, F10.7.

In Figure 3 it is possible to identify several occasions when systematic variations in 40-100 day periods are observed. It is not possible to explain this behavior at the moment, leaving this as a topic for future studies.

5. Acknowledgements

This research was supported by the Finnish Cultural Foundation and the Tauno Tonning Research Foundation. The authors wish to thank Tero Raita for his support in the VLF recordings.

6. References

1. J.R. Wait and K.P Spies, "Characteristics of the Earth-ionosphere waveguide for VLF radio waves", *Volume NBS Technical Note 300. NIST Research Library*, 1964.

2. R.N. Bracewell, et al., "The study of solar flares by means of very long radio waves", *Mon. Not. R. Astron. Soc*., 109, 1949, 28–45, doi: 10.1093/mnras/109.1.28.

3. A. Nina and V.M. Cadez, "Detection of acoustic-gravity waves in lower ionosphere by VLF radio waves", *GRL*, **40**, 2013, pp. 4803-4807, doi: 10.1002/grl.50931.

4. I. Silber, et al., "Semi-annual oscillation (SAO) of the nighttime Ionospheric D-region as detected through ground-based VLF receivers", *Atmos. Chem. Phys.*, **16**, 2016, pp. 3279-3288, doi: 10.5194/acp-16-3279-2016.

5. G. Sharma, et al., "A study on the VLF/LF long term amplitude oscillations associated with frequencies 37.5 kHz and 45.9 kHz received at Keil Longwave Monitor, Keil, Germany", *International J. of Geosciences*, **8**, 2017, pp. 1080-1090. doi: 10.4236/ijg.2017.89061.

6. M. A. Clilverd, et al., "Remote sensing space weather events: Antarctic-Arctic Radiation-belt (Dynamic) Deposition-VLF Atmospheric Research Konsortium network", *Sp Wea.*, **7**, 2009, doi:10.1029/2008SW000412.

7. C. Torrence and G.A. Compo, "practical guide to wavelet analysis", *Bull. of Ame. Met. Soc.*, **79**, 1, 1998.

8. E. Aguilar-Rodriguez, et al., "The wavelet transform function to analyze interplanetary scintillation observations", *GRL*, **41**, 2014, pp. 3331–3335, doi:10.1002/2014GL060047.

9. B. Zieger and K. Mursula, "Annual variation in near-Earth solar wind speed", *GRL*, 25, 1998, pp. 841-844, doi: 10.1029/98GL50414.